Thermochimica Acta 655 (2017) 34–41

Contents lists available at ScienceDirect

Thermochimica Acta

journal homepage: www.elsevier.com/locate/tca

Phase transformation behavior of $Sr_{0.8}Gd_{0.2}CoO_{3-\delta}$ perovskite in the vicinity of order-disorder transition

Sergei N. Vereshchagin[a,*], Vyacheslav A. Dudnikov[b], Nina N. Shishkina[a], Leonid A. Solovyov[a]

[a] Institute of Chemistry and Chemical Technology, 660036 Krasnoyarsk, Russia
[b] Kirensky Institute of Physics, 660036 Krasnoyarsk, Russia

ARTICLE INFO

Keywords:
Perovskite
Ruddlesden-Popper phase
Order-disorder
Phase transition
DSC

ABSTRACT

The phase transformation behavior of a single-phase tetragonal $Sr_{0.8}Gd_{0.2}CoO_{3-\delta}$ (with ordered distribution of Sr^{2+}/Gd^{3+} cations and anion vacancies) was investigated by TG–DSC and XRD at 1100–1473 K and oxygen partial pressure $p(O_2)$ from 1 to $5{\cdot}10^4$ Pa. The first-order smeared order-disorder (o-d) phase transition involving heat absorption was observed at about 1383 K under O_2-Ar flow with $p(O_2) > 2.5$ kPa. The crystal structure of the high-temperature phase was found to be cubic perovskite with disordered Sr^{2+}/Gd^{3+} cations and anion vacancies. The temperature of o-d transition at $p(O_2) > 2.5$ kPa was not influenced by the heating rate or oxygen partial pressure. It was shown that at $p(O_2) < 2.5$ kPa the o-d transition gives rise to $Sr_{0.8}Gd_{0.2}CoO_{3-\delta}$ decomposition to form CoO and $Sr_{2.4}Gd_{0.6}Co_2O_{7-\delta}$ – Ruddlesden-Popper type phase with novel composition. The phase boundaries between the ordered tetragonal $Sr_{0.8}Gd_{0.2}CoO_{3-\delta}$, disordered cubic $Sr_{0.8}Gd_{0.2}CoO_{3-\delta}$ and CoO + $Sr_{2.4}Gd_{0.6}Co_2O_{7-\delta}$ composite as a function of temperature and $p(O_2)$ values were determined.

1. Introduction

Double perovskite oxides $M_xLn_{1-x}CoO_{3-\delta}$ (where Ln is a rare earth element, M is an alkaline earth metal) have been extensively investigated in past decade due to a number of interesting magnetic, optical, transport properties promising for technical applications (magnetic materials, oxygen conducting membrane, electrodes for solid fuel cell, catalysts) [1–6]. This broad diversity of properties is derived not only from the large variety of partially substituted cobaltites but also from different arrangements of A-site cations. It turns out that the A-site La/M distribution has a great influence on physicochemical properties of the $M_xLn_{1-x}CoO_{3-\delta}$ system, such as structure [7], chemical stability, electrical conductivity [8], oxygen stoichiometry and diffusivity [9], magnetic [10] and catalytic properties [11,12].

It is known that $Sr_xLn_{1-x}CoO_{3-\delta}$ perovskites ($0.67 \le x \le 0.9$) containing larger ions La^{3+}, Pr^{3+} and Nd^{3+} display simple cubic structures; compounds containing rare earth ions smaller than Nd^{+3} show a modulated intermediate lattice with a tetragonal superstructure ($I4 = mmm$; $2a_p \times 2a_p \times 4a_p$), coupled Ln/Sr and oxygen/vacancy ordering being responsible for the observed superstructure [7]. At high temperature, the tetragonal perovskites with ordered distribution of Sr^{2+}/Ln^{3+} cations and anion vacancies undergo an order-disorder (o-d) phase transition to a cubic structure with disordered cations/vacancies. For the $Sr_{0.8}Gd_{0.2}CoO_{3-\delta}$ compound, this transition has been shown to occur at 1330–1390 K. The high temperature cubic structure can be quenched as a metastable state, and the catalytic activity of cubic disordered $Sr_{0.8}Gd_{0.2}CoO_{3-\delta}$ in reaction of methane deep oxidation was found to be at least five times greater than that of the ordered tetragonal phase [11,12]. The ordering also results in an anomaly of magnetic behavior near room temperature [10]. Therefore, the formation and stabilization of such partially or completely disordered metastable phases presents a promising way to synthesize advanced perovskite systems with controlled level of disordering which possess new or enhanced properties not inherent to simple perovskites.

At the present time, there is a diversity of data concerning the structure, the physical and chemical properties of ordered/disordered perovskites [13–16] but, to the best of our knowledge, there are no studies describing peculiarities of o-d transition in rare earth perovskites that would allow to control the o-d process. The aim of the present work is to analyze details of temperature- and oxygen-induced transformation of double cobaltite $Sr_{0.8}Gd_{0.2}CoO_{3-\delta}$ in the vicinity of o-d transition.

2. Experimental

Sample of $Sr_{0.8}Gd_{0.2}CoO_{3-\delta}$ was prepared by a conventional solid phase ceramic synthesis from Gd_2O_3, Co_3O_4 and $SrCO_3$ powders (Table 1). Thoroughly weighted amounts of compounds were ground in

* Corresponding author.
E-mail address: snv@icct.ru (S.N. Vereshchagin).

http://dx.doi.org/10.1016/j.tca.2017.06.003
Received 11 April 2017; Received in revised form 5 June 2017; Accepted 8 June 2017
Available online 09 June 2017

Table 1
Summary of sample descriptions.

Chemical Name	Formulae	Source	Purity according to Supplier, %
Cobalt(II, III) oxide	Co_3O_4	Alfa Aesar	99.7[a]
Gadolinium (III) oxide	Gd_2O_3	Alfa Aesar	99.99[a]
Strontium carbonate	$SrCO_3$	Reachim	99.5[a]
Oxygen	O_2	Kriogen	99.95[b]
Argon	Ar	TD Fakel	99.993[b]
Hydrogen	H_2	NCCP	99.99[b]

[a] Mass fraction purity.
[b] Mole fraction purity.

an agate mortar with ethanol, pressed into pellets and calcined at 1473 K for 24 h in air with intermediate re-grinding and re-pelleting. The final ceramic pellets were annealed additionally in air for 24 h and cooled down with cooling rate of 2 K min^{-1}. To ensure the equilibrium oxygen content the sample was kept additionally in air at 773 K for 8 h and cooled down with a ramp rate of 2 K min^{-1} prior to DSC measurements.

X-ray powder diffraction data (XRPD) were collected on a PANalytical X'Pert PRO diffractometer equipped with a solid-state detector PIXcel and graphite monochromator on Cu K_α radiation over the 2θ range 5–110°. An Anton Paar HTK 1200N high-temperature camera with the sample rotation and automated alignment was used. Powder samples were prepared by grinding with octane in an agate mortar and packed into a flat sample holder for the diffraction measurements in the Bragg-Brentano geometry. The full-profile crystal structure analysis was done using the Rietveld method with the derivative difference minimization refinement [17].

The oxygen nonstoichiometry δ of initial $Sr_{0.8}Gd_{0.2}CoO_{3-\delta}$ was calculated from the results of the thermogravimetric reduction [18], assuming that the cobalt is reduced to the metallic state (Eq. (1)). The amount of oxygen (δ) consumed/released during the cooling/heating cycles was calculated from the mass variation.

$$Sr_{0.8}Gd_{0.8}CoO_x + (x - 1.4)\ H_2 = 0.4\ Gd_2O_3 + 0.2\ SrO + Co + (x - 1.4)\ H_2O \quad (1)$$

The reduction was performed on a NETZSCH STA 449C analyzer in a stream of argon with 5% H_2, heating the samples up to 1173 K with a rate of 10 K min^{-1}. The reduction process was carried out in Al_2O_3 crucibles with percolated lid, a sample mass of 22 ± 0.5 mg. The measurements were carried out with correction for the buoyancy force, i.e. blank experiments (base line) have been performed at the same conditions with empty crucibles.

STA experiments were performed on a TG-DSC NETZSCH STA 449C analyzer equipped with an Aeolos QMS 403C mass spectrometer. The measurements were carried out under dynamic O_2-Ar atmosphere at ambient pressure (1.01-1.04)·10^5 Pa) in crucibles with perforated lids made of Al_2O_3 (ΔH determination) or Pt (variable oxygen partial pressure $p(O_2)$ or ramp rates). For DSC experiments a monolith polycrystalline sample 1.5 × 2 × 1 mm (16 mg) was used. Various $p(O_2)$ were prepared by mixing Ar and O_2 + Ar flows, the oxygen content (partial pressure) in the flows was determined by on-line QMS in the Multiple Ion Detection mode from intensity of ion $m/z = 32$, the purity of the gases used are summarized in Table 1.

The sensor sensitivity was calibrated via C_p measurements of the sapphire disk [19] and crosschecked by measuring Au (NETZSCH standard, T_m = 1335.2 K, ΔH = 63.7 Jg^{-1}), relative expanded uncertainty with 0.95 level of confidence U_r (coverage factor $k = 2$) of ΔH determination was 0.04.

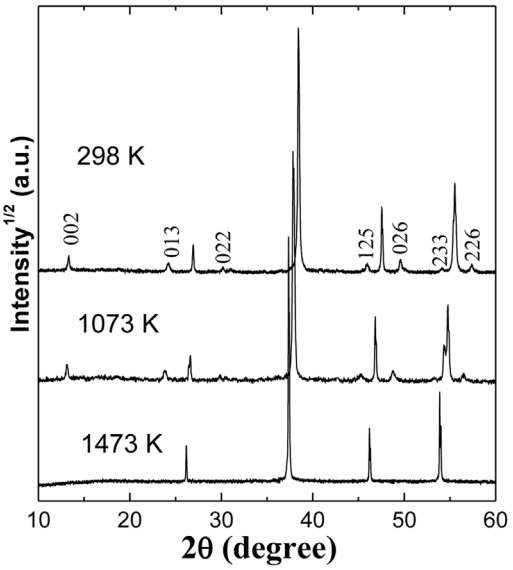

Fig. 1. Characteristic XRD pattern fragments of $Sr_{0.8}Gd_{0.2}CoO_{3-\delta}$ in air at 298, 1073 and 1473 K. Superstructure peaks of tetragonal ordered phase are indexed.

3. Results and discussion

3.1. Structure of ordered and disordered $Sr_{0.8}Gd_{0.2}CoO_{3-\delta}$

The Sr-Gd double cobaltite annealed from 1473 K and equilibrated with air at 773 K has composition $Sr_{0.8}Gd_{0.2}CoO_{2.63}$ (δ = 0.37) and XRD pattern of the sample thus prepared (Fig. 1) corresponded well to the *I4/mmm* superstructure with ordered Gd/Sr sites and anion vacancies (Fig. 2a) [7]. In this structure there are three distinct crystallographic positions which can accommodate Gd^{3+} or Sr^{2+} ions and four positions for O^{2-}. Two of these A-sites (A2–A3) are occupied exclusively by Sr^{2+} (Fig. 2, a; shown as green spheres) while the remaining site (A1, shown as magenta spheres) may contain both Gd^{3+} and Sr^{2+} ions. The regular alternations of pure Sr^{2+} positions in the ordered state are accompanied, as well, by regularities in the distribution of oxygen vacancies (which are located in O2-sites) and CoO_6 octahedra tilting. In the disordered $Sr_{0.8}Gd_{0.2}CoO_{2.51}$ (1447 K) or quenched $Sr_{0.8}Gd_{0.2}CoO_{2.71}$ all A-sites are equivalent and occupied by either Gd^{3+} or Sr^{2+} in a random order (Fig2, b; magenta spheres). Oxygen vacancies are randomly distributed over the respective O-sites.

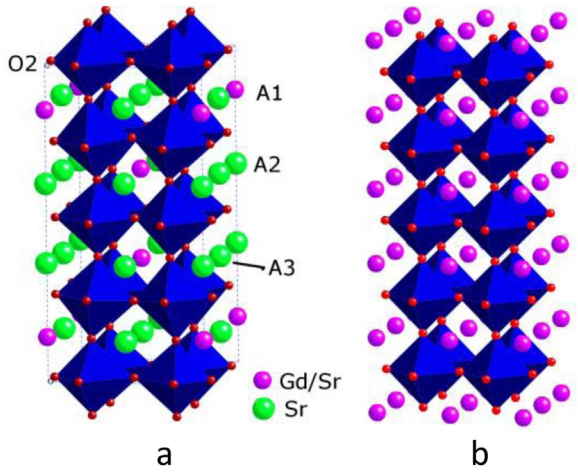

Fig. 2. The structure of ordered (a) and disordered (b) $Sr_{0.8}Gd_{0.2}CoO_{3-\delta}$. Blue octahedra represent Co, green spheres represent Sr, magenta spheres represent Gd/Sr and smaller red spheres are oxygen. (For interpretation of the references to colour in this figure legend, the reader is referred to the web version of this article.)

Table 2
Crystal structure parameters of compound under investigation.

Phase	Design-ation	T, K	State	Crystal cell	Space group	*a*, nm***	*c*, nm***
$Sr_{0.8}Gd_{0.2}CoO_{2.63 \pm 0.01}$	o-P	298	ordered	tetragonal	*I4/mmm*	0.7692 (3)	1.5321(8)
$Sr_{0.8}Gd_{0.2}CoO_{2.71 \pm 0.01}$	d-P	298	disordered*	cubic	*Pm3m*	0.38342(1)	
$Sr_{0.8}Gd_{0.2}CoO_{2.51 \pm 0.01}$		1473	disodered	cubic	*Pm3m*	0.39464(1)	
$Sr_{2.4}Gd_{0.6}Co_2O_{6.23 \pm 0.02}$**	n = 2-RP	298		tetragonal	*I4/mmm*	0.38541(2)	1.9929(1)
CoO	CoO	298		cubic	*Fm3m*	0.42605(2)	

* Quenched from 1473 K.
** δ determined from TG data, see *Supplemental files*.
*** Estimated standard uncertainties are given in parentheses.

Crystallographic parameters of $Sr_{0.8}Gd_{0.2}CoO_{3-\delta}$ phases are summarized in Table 2.

3.2. Observation of phase transition of $Sr_{0.8}Gd_{0.2}CoO_{3-\delta}$ by TG-DSC

When heated in O_2-Ar flow ($p(O_2)$ = 20.3 kPa) $Sr_{0.8}Gd_{0.2}CoO_{2.63}$ started losing oxygen at about 773 K with the gradual mass decrease (Fig. 3) and a pronounced *endo*-effect was observed at 1343–1400 K with increasing temperature (T_{min} = 1383 ± 0.5 K, ΔH = 16.4 ± 3.1 Jg^{-1}, expanded uncertainty with 0.95 level of confidence). The high-temperature in situ XRD analysis showed that above 1400 K the superstructure reflections disappeared (Fig. 1) indicating a transformation to fully disordered cubic perovskite phase (Fig. 2b) with $Sr_{0.8}Gd_{0.2}CoO_{2.51}$ composition (at 1473 K). Being quenched from this temperature in air the sample retains a cubic structure (Fig. 1).

During cooling from 1473 K a distinct exotermal peak was observed in the DSC curve at 1354–1253 K (T_{max} = 1332 K) against the background of the progressive mass increase (Fig. 3) pointing out a reversible character of the transformation. The reversibility is corroborated by the restoration of superstructure reflections after a slow cooling from 1473 K to room temperature. It should be noted that TG-curves for heating/cooling cycles almost coincide testifying a high oxygen mobility and an identical stoichiometry δ. Thus, one may ascribe the observed DSC effects to the cation/anion vacancies order–-disorder (o-d) phase transition.

There was no appreciable mass change observed at the point of o-d transition (Fig. 3) and this is different from behavior of other perovskite systems, in particular, iron compound $Ba_2Fe_2O_{5+\delta}$ display an abrupt mass increase in the TG curve at the point of first order phase transition from the ordered oxide ion vacancies in monoclinic $Ba_2Fe_2O_5$ to the disordered ones in the cubic perovskite [20]. In our case only slopes of dm/dT curves (Fig. 3) before and after o-d transition were slightly different in agreement with an enhanced oxygen mobility in the cubic disordered perovskite $Sr_{0.8}Gd_{0.2}CoO_{3-\delta}$ compared to the ordered tetragonal one [11].

A hysteresis clearly observed in DSC peaks for the heating-cooling cycle (Fig. 3) may indicate that the anomaly of the DSC curves corresponds to the first-order phase transition. But it is known that a peak position in DSC curves (including T_{max} and T_{min}) may contain a methodological error due to the thermal resistance of the sensor-crucible-sample system. To eliminate this error a special procedure [21] was employed in which T_{min} and T_{max} values of DSC peaks obtained at different heating/cooling rates β were plotted versus $\beta^{1/2}$ to produce straight lines. Extrapolation of these linear relations to $\beta = 0$ yields the true phase transition temperatures not distorted by methodological errors.

Fig. 4 shows a set of DSC curves recorded at 2.5–20 K min^{-1} scanning rates and $T_{min,max} = f(\beta^{1/2})$ plot. It is evident from Fig. 4 that substantial hysteresis observed at β = 0 let us assigns o-d transformation to a first order phase transition.

It is interesting that T_{max} and half-width of DSC peaks for the formation of the ordered phase (d-o transformation) depend on the β-value while the ramp rate β does not affect the position of endothermic DSC peaks of disordering process. Moreover, the constant contour of DSC-signal and invariability of the half-width on β (ΔT is about 20 K for all endothermic peaks) allow asserting that order-to-disorder transformation of $Sr_{0.8}Gd_{0.2}CoO_{3-\delta}$ at 1383 K is controlled by thermodynamic parameters rather than by kinetics of nucleation and this process is smeared by temperature. The occurrence of the structural transformation in the temperature range is typical of "so-called" smeared (diffused) phase transitions and results in characteristic peak-like anomalies in the temperature dependences of crystal properties such as heat capacity [22,23], dielectric permittivity [24] and some others.

The origin of the smearing of phase transitions is supposed to be connected with the influence of fluctuations of composition or structural defects concentration on the critical temperature, which fluctuates

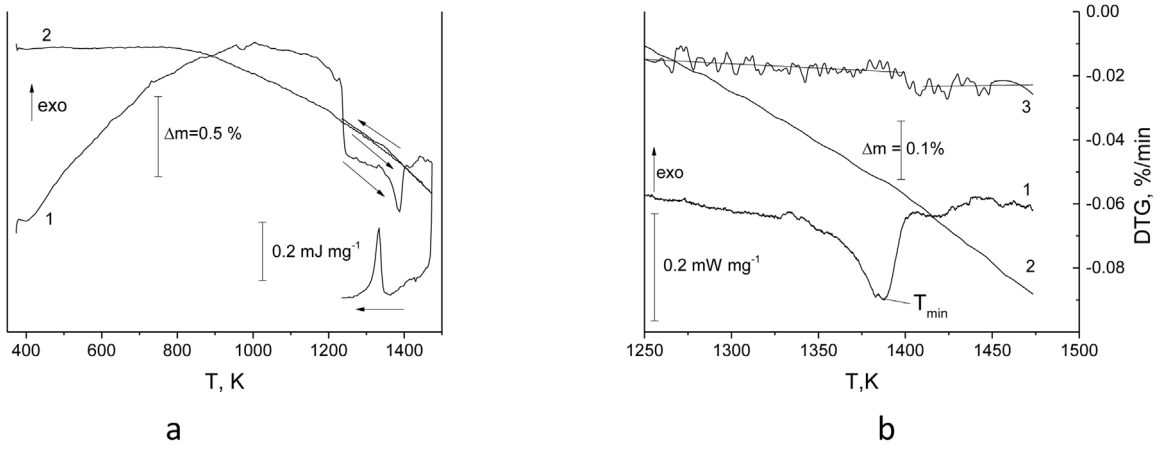

Fig. 3. a – DSC(1) and TG(2) signals for $Sr_{0.8}Gd_{0.2}CoO_{2.63}$ under O_2-Ar flow ($p(O_2)$ = 20.3 kPa). Heating to 1233 K, β = 20 K min^{-1}, then heating to 1473 K and cooling to 1233 K, β = 10 K min^{-1}. Arrows show direction of temperature changes. b – DSC (1),TG (2) and DTG (3) signals in the vicinity of phase transition temperature. Straight lines are guides for eyes to monitor dm/dT changes.

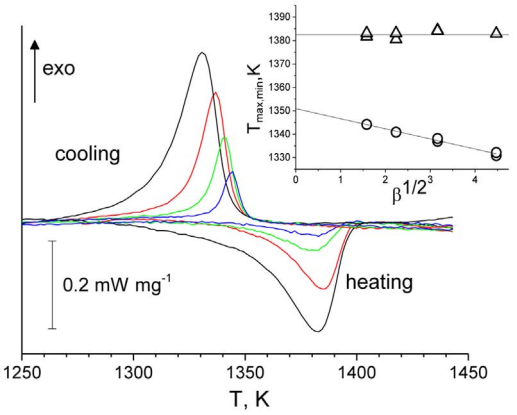

Fig. 4. Heating-cooling DSC curves for $Sr_{0.8}Gd_{0.2}CoO_{3-\delta}$, O_2-Ar flow ($p(O_2) = 20.3$ kPa); β = 2.5 (blue), 5 (green), 10 (red) and 20 (black) K min^{-1}. The inset shows T_{min} (endo) and T_{max} (exo) as a function of $\sqrt{\beta}$; Δ − heating, ○ − cooling. (For interpretation of the references to colour in this figure legend, the reader is referred to the web version of this article.)

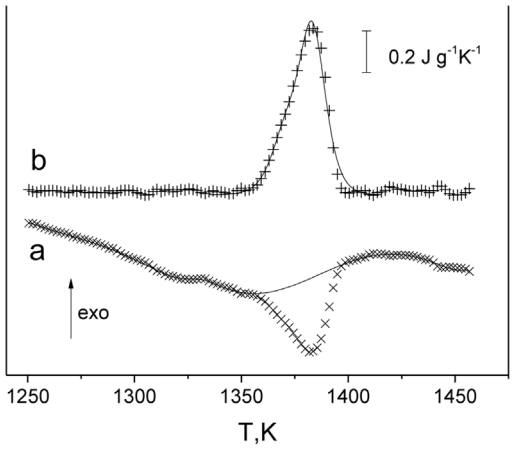

Fig. 5. a − DSC signal (×) and baseline correction (line) for anomalous ΔC_p calculation, $\beta = 10$ K min^{-1}, 20% O_2-Ar; b − experimental (+) and theoretical (line) temperature dependence of ΔC_p for o-d phase transition of $Sr_{0.8}Gd_{0.2}CoO_{3-\delta}$.

about the mean phase-transition temperature [25,26]. The second viewpoint is based on assumption that smearing of phase transitions is caused by a cooperative motion of atoms associated with the motion of interphase boundaries. The change of mobility of interphase boundaries due to their interaction with structural defects results in the variation of temperature range of the transformation. These hypotheses were used to develop the phenomenological theory of smeared phase transitions [27] which allows to describe quantitatively Λ-shaped peaks in the temperature dependences of the crystal properties. According to this theory, the temperature dependence of the anomalous heat capacity associated with phase transition can be represented by Eq. (2)

$$\Delta C_p(T) = \Delta C_{p,m} \frac{4\exp\left(B\left(\frac{T}{T_0} - 1\right)\right)}{\left(1 + \exp\left(B\left(\frac{T}{T_0} - 1\right)\right)\right)^2} \quad (2)$$

$$B = \frac{\omega \rho q_0}{k T_0} \quad (3)$$

$$\Delta C_{p,m} = \frac{B q_0}{4 T_0} \quad (4)$$

Where$T$ − temperatureT_0 − characteristic temperature, at which ratio of high to low temperature phase is unity$\Delta c_{p,m}$ − maximum heat capacity at $T = T_0 B$ − athermal parameterω − elementary volume of the transformationq_0 − heat of transformation$k$ − the Boltzmann constantρ- crystal density

The Eq. (3) contains a parameter ω − elementary volume which relates to the mechanism of the phase transition. It corresponds to the certain volume of existing phase where different fluctuations are localized and growth of the new phase occurs by addition of a small volume ω to phase boundary, ω value depending on defect concentration. This approach was used to characterize ferroelectric materials where the elementary volume of the phase transformation was shown to be comparable to the volume of the Känzig region [28,29], to determine the number of molecules involved in the elementary act of correlated transformation of C_{60}-crystals during the orientational structural transformation at 250–260 K [27] to elucidate texture dependent peculiarities of first-order phase transition at 240–260 K in $Sm_{1+x}S$ [23].

It has been shown above (Fig. 4) that DSC peak profiles for disordering process do not depend on experimental condition and are determined most probably by thermodynamic factors. It allows one to apply the theory of smeared phase transitions to the o-d transformation of $Sr_{0.8}Gd_{0.2}CoO_{3-\delta}$. To perform this a heat capacity ΔC_p associated with the transition was isolated from the total DSC signal by subtracting the baseline (DSC trend, Fig. 5a) and recalculating the profile to C_p-scale: $\Delta C_p = \Delta DSC[J\ s^{-1} g^{-1}]/\beta[K\ s^{-1}]$ (Fig. 5). Temperature dependence of ΔC_p obtained under heating at the scanning rate of 10 K min^{-1} exhibits an asymmetric peak with a poorly defined low temperature shoulder (Fig. 5b). This suggests a complex character of the transformation process, which evidently cannot be described by Eq. (2). As it follows from thermodynamic approach based on the self-consistent field model [30], such kind of the asymmetric broadening of the property-temperature curve is inherent to phase transitions of intermediate types between the first-order and second-order phase transitions [27].

A close look at the structure difference between ordered and disordered $Sr_{0.8}Gd_{0.2}CoO_{3-\delta}$ allows suggesting an alternative explanation. In fact the o-d transformation includes two disordering processes: (i) spreading of oxygen vacancies which are located in O2-site in the ordered structure throughout the crystal and (ii) redistribution of Sr^{2+}/Gd^{3+} cation over A-sites in a random order. If these processes are partially independent then one may observe ether broadening or even two overlapping peaks.

The tendency for A-site cations to order is considered to originate from the bond strains, the bonding instabilities created by ordering are generally compensated either by anion vacancies or second order Jahn–Teller distortions of a B-site cation [31]. The absence of rigid correlation between o-d behavior of anionic and cationic sublattice is illustrated by the results of $La_{0.1}Sr_{0.9}Co_{0.9}Fe_{0.1}O_{3-\delta}$ study [16] where transition of brawnmillerite to disordered perovskite (i.e. oxygen vacancies randomization) occurred without changes in the cationic sublattice. An additional argument of relative independence of these two processes is the observation that in $Ln_{1-x}Sr_xCoO_{3-\delta}$ (Ln = La^{3+}, Pr^{3+} and Nd^{3+}; x > 0.60) oxygen vacancy ordering was not accompanied by additional Ln^{3+}/Sr^{2+} cation redistribution [32].

If this assumption is true in our case then the observed DSC endoeffect is a result of two transformations which are shifted by temperature to each other and the profile of anomalous heat capacity ΔC_p can be expressed as a superposition of corresponding dependencies. Fig. 5 shows approximation of experimental ΔC_p values by a function $\Delta C_p = \Delta C_{p1} + \Delta C_{p2}$, where ΔC_{p1} и ΔC_{p2} are defined by Eq. (2). It is obvious that the equation describes quite accurately the temperature dependence of ΔC_p. Parameters of the model and their expanded uncertainties with 0.95 level ofconfidence were estimated by nonlinear least-squares regression: $B_1 = 295 \pm 32$, $C_{p,m1} = 0.27 \pm 0.11$ J $g^{-1}K^{-1}$, $T_1 = 1371 \pm 2$ K and $B_2 = 338 \pm 50$, $C_{p,m2} = 0.78 \pm 0.12$ J $g^{-1}K^{-1}$, $T_2 = 1383 \pm 1$ K. Given the density of perovskite crystal $\rho = 5.53$ g cm^{-1} (at 1380 K) and combining Eqs. (3) and (4) we can determine an elementary volume of the transformation from the relationship $\omega = kB^2/(4\rho\Delta C_{p,m})$ as follows:

ω_1 = 200 nm^3 and ω_2 = 90 nm^3. The lattice parameters for tetragonal $Sr_{0.8}Gd_{0.2}CoO_{2.63}$ are a=0.7692 nm and c=1.532 nm (Table 2), thus the number of elementary cells involved in the act of correlated transformation can be estimated as $n = \omega/V$=100-220. The peak at 1371 K is likely to correspond to oxygen vacancies disordering whereas that at 1383 K can be ascribed to cation randomization. For this model we can estimate from Eq. (4) heats of transformations $q_0 = 4T_0\Delta c_{p,m}/B$: q_1=5.0 Jg^{-1} and q_2=12.7 Jg^{-1} which are in sufficiently good agreement with the total enthalpy of the phase transition ΔH=16.4 ± 3.1 Jg^{-1}.

3.3. Effect of $p(O_2)$ on phase transitions of $Sr_{0.8}Gd_{0.2}CoO_{3-\delta}$

Fig. 6a shows DSC curves of $Sr_{0.8}Gd_{0.2}CoO_{3-\delta}$ under O_2-Ar mixtures with $p(O_2)$ values ranged from 100 Pa to 51 kPa. To study effects of p (O_2) on phase conversion the following temperature program was employed: a sample was kept at 1233 K for 1 h, then heated to 1473 K and cooled to 1233 K with a rate of 10 K min^{-1}.

In the heating curves no significant variation of T_{min}=1383 K was found for $p(O_2)$=5–50 kPa. It is in accord with the observation that no oxygen release occurs during the phase transition (Fig. 3b) and that the disordering process is controlled thermodynamically. As opposed to this the $p(O_2)$ variation results in a shift of T_{max} values in the cooling DSC curves (Fig. 6a), the decrease of $p(O_2)$ from 50 to 5 kPa leading to the increase of T_{max} from 1323 to 1341 K. This behavior can be a consequence of the increase of the anion vacancies concentration which facilitate A-site cation ordering as it was proposed in $LnBaM_2O_{5+\delta}$ [31]. Though the thermogravimetric analysis demonstrated that a critical level of oxygen vacancies in $La_{0.5}Ba_{0.5}CoO_{3-\delta}$ is required in order to stabilize the A-site cation ordered structure [8] no clear dependence is observed between the position of T_{min} of disordering and δ for the studied sample $Sr_{0.8}Gd_{0.2}CoO_{3-\delta}$ (Fig. 6a, inset).

A different behavior is observed when a flow of argon ($p(O_2)$ =180 Pa) was used instead of O_2-Ar mixture. Under these conditions, position of the DSC peak is sensitive to the oxygen content (Fig. 6). The reduction of $p(O_2)$ leads to the parallel decrease of T_{mim} under heating and results in substantial drop of T_{max} in cooling curves. Additionally an abrupt mass decrease occurs along with DSC *endo*-effect due to the oxygen release which is detected by mass-spectrometer (Fig. 6b).

The XRD pattern of the sample treated in an oxygen depleted atmosphere does not reveal the presence of perovskite $Sr_{0.8}Gd_{0.2}CoO_{3-\delta}$ (Fig. 7a). Instead, two crystalline phases were detected: 87 wt.% of nonstoichiometric tetragonal phase which belongs to Ruddlesden-Popper family (n=2-RP) and 13 wt.% of cubic CoO. Thus, we can affirm that $Sr_{0.8}Gd_{0.2}CoO_{3-\delta}$ is unstable under this condition and undergoes decomposition to form n=2-RP + CoO composite according to an Eq. (6). After complete conversion of $Sr_{0.8}Gd_{0.2}CoO_{3-\delta}$ the theoretical content of CoO in $Sr_{2.4}Gd_{0.6}Co_2O_{7-\delta1}$ + CoO composite is 12.5% (assuming δ_1=0.77, see *Supplemental files*) which is in good agreement with 13% found from XRD data. SEM images show that CoO phase is included in the body of $Sr_{2.4}Gd_{0.6}Co_2O_{7-\delta1}$ as 1-2 μm domains (Fig. 1S, *Supplemental files*) clearly detectable by energy-dispersive X-ray analysis. It is interesting to note that the reaction is reversible and $Sr_{2.4}Gd_{0.8}Co_2O_{7-\delta1}$ + CoO composite turns into the perovskite $Sr_{0.8}Gd_{0.2}CoO_{3-\delta}$ when $p(O_2)$ is increased. The full-profile XRPD refinement of $Sr_{2.4}Gd_{0.6}Co_2O_{7-\delta1}$ structure using the Rietveld method with the derivative difference minimization (DDM) [17] gave the following crystal lattice parameters: $a = b$ = 0.38541(2), c = 1.9929(1) nm, V = 0.29602(4) nm^3, Z = 2, space group *I4/mmm* (Fig. 7b, Table 2).

To the best of our knowledge the transformation of Sr-rich Sr-Gd-Co perovskite to n=2-RP phase of $Sr_{2.4}Gd_{0.8}Co_2O_{7-\delta1}$ composition has not been described in literature yet but it is well known that double perovskites $M_xLn_{1-x}CoO_{3-\delta}$ (where Ln is a rare earth element, M is an alkaline earth metal) are unstable under a reducing or oxygen-depleted atmosphere and decomposed to give RP phases. The phase equilibria in the Ln–Co–O and Ln–M–Co–O system have been studied in detail and results are summarized in a number of reviews [33] and references presented therein]. In particular, cobaltites can decompose to different members of PR family depending on composition, temperature, $p(O_2)$. It was shown that $La_{0.7}Sr_{0.3}Co_{3-\delta}$ decomposes to $(La_{0.7}Sr_{0.3})_2CoO_{4-\delta}$ + $Co_{1-\gamma}O$ at 1383 K and log(P_{O2},atm) = −2.8 [34]; $LaCoO_3$ sequentially undergoes transformation to $La_4Co_3O_{10}$ and La_2CoO_4 when decreasing $p(O_2)$ [35].

Numerous studies have shown that the crystal structure of RP compounds consists of an intergrowth of single AO rock salt (RS) layers with multiple perovskite (P) layers, according to the formulation $AO(ABO_3)_n$, which gives rise to a row of compounds such as A_2BO_4 (n = 1), $A_3B_2O_7$ (n = 2, Fig. 7b) …. ABO_3 (n = ∞). In the case of double perovskites (A = Ln/M) Ln^{3+} and M^{2+} ions tend to order in RS and P layers along c axis. It was shown that Ruddlesden-Popper stoichiometric $Gd_{2-2x}Sr_{1+2x}Co_2O_7$ compounds (x = 0 and 0.10) present the ordering of A-site cations where the bigger Sr^{2+} cation selectively prefers the 12-coordinated site located within the perovskite-like layers (P) while the smaller Gd^{3+} cation prefers the 9-coordinated site, located within the rock-salt-like layers (RS) [36]. An opposite Ln^{3+}/Sr^{2+} distribution was found in phase $SrTb_2Fe_2O_7$ where the structure is formed by the adjunction of two perovskite cells with Tb^{3+} cations and the other one by a halved RS-SrO cell [39]. A very limited information is available on the cation distribution in the oxygen-deficient cobaltites $A_3Co_2O_{7-\delta}$ with A = Sr, Ln [37]. For instance,

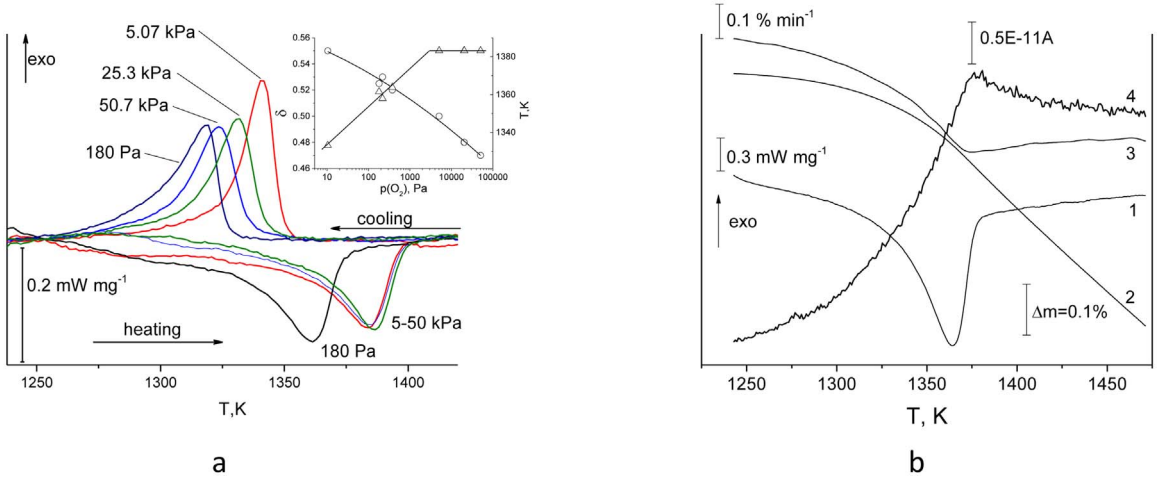

Fig. 6. a- heating-cooling DSC curves for $Sr_{0.8}Gd_{0.2}CoO_{3-\delta}$ under different oxygen partial pressure, curves are labeled with $p(O_2)$, β = 10 K min^{-1}; inset − variation of T_{min} of endoeffect (Δ) and δ (○, calculated at T_{min}) as a function of $p(O_2)$. b − DSC (1), TG (2), DTG (3) signals and intensity of ion m/z=32 (4) as a function of temperature in the vicinity of phase transition. $p(O_2)$ = 375 Pa, β = 10 K min^{-1}.

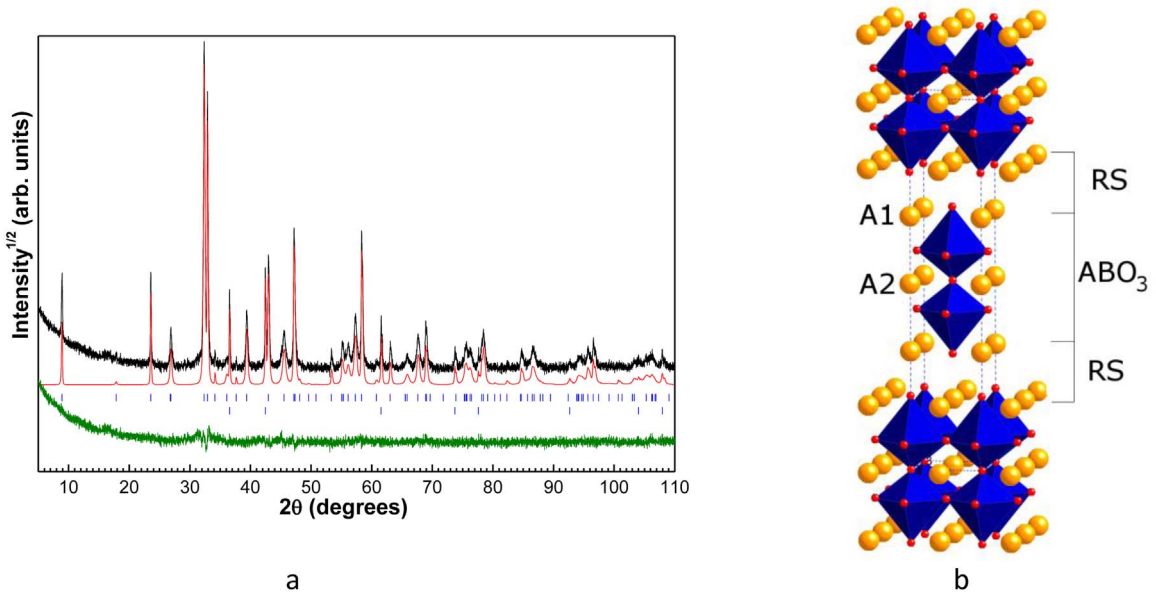

Fig. 7. a − Observed (top), calculated (middle) and difference (bottom) XRPD profiles after DDM refinement. Calculated peak positions of $Sr_{2.4}Gd_{0.6}Co_2O_{7-\delta}$ and CoO are marked by ticks. b − crystal structure of $Sr_{2.4}Gd_{0.6}Co_2O_{7-\delta}$. Blue octahedra represent Co, orange spheres represent A-sites and smaller red spheres are oxygen. (For interpretation of the references to colour in this figure legend, the reader is referred to the web version of this article.)

$Sr_2Y_{0.8}Ca_{0.2}Co_2O_6$ crystallizes in the tetragonal I4/mmm space group and displays an ordering of Sr^{2+} and Y^{3+}/Ca^{2+} species, the smaller cations Y^{3+}/Ca^{2+} sitting inside the double pyramidal cobalt layers [38].

In our case preliminary data indicate that Gd^{3+}/Sr^{2+} cations also show a preference for distinct sites in the oxygen-deficient structure of synthesized $Sr_{2.4}Gd_{0.6}Co_2O_{7-\delta 1}$, the A-site cations and anion vacancies arrangement strongly depending on the synthesis conditions. Details of this influence are a subject of a separate structural study which is well under way and will be published soon.

3.4. Phase boundary between ordered/disordered $Sr_{0.8}Gd_{0.2}CoO_{3-\delta}$ and $Sr_{2.4}Gd_{0.6}Co_2O_{7-\delta}$ + CoO

The aim of the present paper was not to draw a phase diagram of the system; instead the goal was to elucidate the condition of the phases inter conversion enabling the generation of new states, which can, in turn, lead to improved performance and new functionalities. To perform the task a number of DSC runs were carried out under different experimental condition and results are summarized in Fig. 8. In the figure the points marked (■) were obtained by heating o-P from 1233 to 1473 K ($\beta = 10$ K min^{-1}) after 1 h equilibration at 1233 K and constant $p(O_2)$ ranged from 1 to $5{\cdot}10^4$ Pa. Two trends of $ln p(O_2)$-$1/T_{min}$ dependences become apparent from the data. The fist one at $p(O_2) > 5$ kPa is a result of the reversible smeared phase o-d transition (Eq. 5), temperature of the transformation being independent on $p(O_2)$. The second trend at $p(O_2) < 1.6$ kPa corresponds to the disordering of o-P with the subsequent or parallel conversion to $n = 2\text{-RP} + CoO + O_2$ (Eq.6). A linear correlation is observed between $ln p(O_2)$ and $1/T_{min}$ under the oxygen-depleted atmosphere (Fig. 8) and the o-P transformation seems to proceed without distinct separation of disordering/decomposition processes because there was only one pronounced *endo*-peak in the DSC heating curve under experimental condition applied. An intersection of the regression lines (a point marked ○) gives $p(O_2) = 2.7$ kPa which can be considered as a stability limit of o/d-$Sr_{0.8}Gd_{0.2}CoO_{3-\delta}$ towards decomposition.

$$o\text{-}Sr_{0.8}Gd_{0.2}CoO_{3-\delta}\ (\text{tetragonal}) \rightleftharpoons d\text{-}\ Sr_{0.8}Gd_{0.2}CoO_{3-\delta}\ (\text{cubic}) \quad (5)$$

$$3\ Sr_{0.8}Gd_{0.2}CoO_{3-\delta}\ (\text{tetragonal/cubic}) \rightleftharpoons Sr_{2.4}Gd_{0.6}Co_2O_{7-\delta 1} + CoO + 0.5(1-3\delta+\delta_1)\ O_2 \quad (6)$$

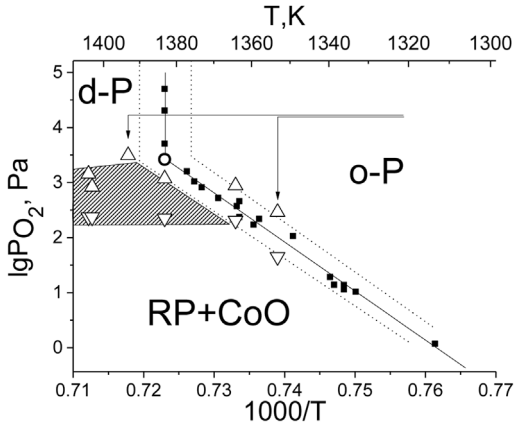

Fig. 8. Phase boundary of tetragonal ordered (o-P), cubic disordered (d-P) $Sr_{0.8}Gd_{0.2}CoO_{3-\delta}$ and $Sr_{2.4}Gd_{0.6}Co_2O_{7-\delta}$ + CoO composite (RP + CoO). Points (■) show T_{min} of DSC peaks, dotted line designates region of smeared phase transition. Triangles stand for $p(O_2)$ at onset (Δ) and minimum (▽) of DSC peaks, obtained in isothermal conditions under programmed $p(O_2)$ reduction, a polygon marks region of d-P to RP + CoO transformation.

To find out the condition of d-P to $n = 2\text{-RP} + CoO + O_2$ transformation the following procedure was utilized. A sample of o-P was subjected to 16 kPa O_2, equilibrated for 1 h at 1233 K, then heated to the predefined temperature T_{fin} = 1353–1403 K and purged for 5 min. After that $p(O_2)$ was gradually reduced by changing the mixing ratio of Ar and O_2-Ar MFC flows. Arrows in Fig. 8 show the temperature − $p(O_2)$ trajectories for T_{fin} 1353 and 1393 K.

The resulting DSC curves consist of one or two *endo*-effects depending on the T_{fin} temperature. For $T_{fin} >$ 1383 K two peaks are observed: the first one at 1383 K for o-d transition is situated in the heating segment of the run; the second one becomes apparent in isothermal segment during $p(O_2)$ reduction step (Fig. 9a). Only one pronounced *endo*-effect is observed for $T_{fin} <$ 1383 K (Fig. 9b). The $p(O_2)$ values at extrapolated onset of DSC peaks satisfy relatively good the proposed borderline of smeared phase transition in this temperature interval and those at minimum of DSC peaks lie slightly below the regression line $p(O_2)$-$1/T_{min}$ (Fig. 8). This shift can be attributed most probably to the kinetics of perovskite decomposition process.

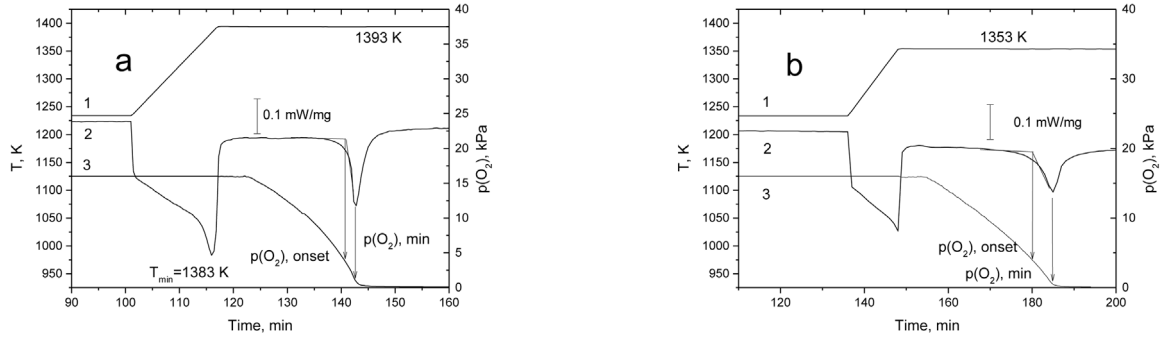

Fig. 9. Temperature (1) and $p(O_2)$ (2) profiles applied and DSC curve obtained (3) under thermal analysis with $p(O_2)$ variation at 1392 K (a) and 1353 K (b).

Unfortunately, we fail to determined clearly the defined borderline for the transformation of d-P to n = 2-RP + CoO composite; the values of $p(O_2)$ at onset and minimum of DSC peaks varied within significant limits depending on experimental conditions: initial oxygen partial pressure, rate of $p(O_2)$ reduction, T_{fin} and temperature ramp rate β. A filled polygon in Fig. 8 shows the region of the transformation (according to the DSC data) for initial $p(O_2) = 16$ kPa. It is interesting that at 1383 K and ~2.7 kPa (the point marked ○, Fig. 8) one can expect coexistence of all phases (namely o/d P, n = 2-RP, CoO and gaseous O_2). Formally speaking, if we consider for this point an equilibrium then according to the Gibbs phase rule for multicomponent systems (the species approach), there are four species Sp ($Sr_{0.8}Gd_{0.2}CoO_{3-\delta}$, $Sr_{2.4}Gd_{0.6}Co_2O_{7-\delta 1}$, CoO, O_2), one relation r (for reaction equilibrium) and five phases Ph (o-P(s), d-P(s), n = 2-RP(s), CoO(s), gas phase). The phase rule gives a number of degrees of freedom $F = 2 + Sp - r - Ph = 2 + 4 - 1 - 5 = 0$ and therefore it corresponds to an invariant point. Of course, there cannot be a true equilibrium for four solid phases, rather, the phases are in mechanical (kinetic) equilibrium but the behavior of the system near this point assumes that no independent changes in the state of the system can be made.

The results presented in Fig. 8 show how different combinations of coexisting phases can be achieved by varying $p(O_2)$ and temperature; the subsequent quenching of these states enable one to stabilize unusual ordered/disordered states or composites which can display properties not inherent to parent compounds.

4. Conclusions

The studied Sr-Gd cobaltite displays the complex phase behavior in the vicinity of point of the order-disorder phase transition. Under oxygen rich atmosphere tetragonal ordered $Sr_{0.8}Gd_{0.2}CoO_{3-\delta}$ undergoes the reversible first order phase transition, the disordering process being smeared by the temperature and controlled by thermodynamic factors while the reverse ordering transformation being controlled kinetically. Under oxygen depleted atmosphere both ordered and disordered phases are unstable; in the case of o-$Sr_{0.8}Gd_{0.2}CoO_{3-\delta}$ o-d transition is complicated by the decomposition of perovskite phase giving a composite of CoO and $Sr_{2.4}Gd_{0.6}Co_2O_{7-\delta}$ − a nonstoichiometric phase which belongs to the Ruddlesden-Popper family $AO(ABO_3)_2$ with the novel composition. There was no distinguished boundary found for d-$Sr_{0.8}Gd_{0.2}CoO_{3-\delta}$ to CoO + $Sr_{2.4}Gd_{0.6}Co_2O_{7-\delta}$ conversion, instead a broad field in *lg* $p(O_2)$-1/T diagram corresponds to conditions of the transformation. Based on these results, novel synthetic routes for perovskite systems can be envisaged, enabling the design of partially disordered materials with new functionalities and improved performance. Such routes are not limited to precise control of cation and anion vacancies disordering process, but can be used also to prepare nanoscaled multiphase ceramic composites comprised of metal oxides and perovskite or perovskite-like phases. This kind of material is known to be of interest for photocatalytic water decomposition [40] or solid oxide fuel cells due to enhancement of oxygen surface-exchange properties [41].

Acknowlegments

The reported study was funded by Russian Foundation for Basic Research, Government of Krasnoyarsk Territory, Krasnoyarsk Region Science and Technology Support Fund to the research project #16-43-240505 p_a and #16-02-00507A.

Appendix A. Supplementary data

Supplementary data associated with this article can be found, in the online version, at http://dx.doi.org/10.1016/j.tca.2017.06.003.

References

[1] S.W. Tao, J.T.S, Irvine Metal Oxides: Chemistry and Applications, in: J.L.G. Fierro (Ed.), CRC Press, Boca Raton, 2006(P. 739).
[2] T. Inagaki, K. Miura, H. Yoshida, R. Maric, S. Ohara, X. Zhang, K. Mukai, T. Fukui, High-performance electrodes for reduced temperature solid oxide fuel cells with doped lanthanum gallate electrolyte: II La(Sr)CoO_3 cathode, J. Power Sources 86 (2000) 347–351.
[3] C.H. Chen, H.J.M. Bouwmeester, R.H.E. Doorn, H. Kruidhof, A.J. Burggraaf, Oxygen permeation of $La_{0.3}Sr_{0.7}CoO_{3-\delta}$, Solid State Ionics 98 (1997) 7–13.
[4] C.R. Michel, A.H. Martínez, F. Huerta-Villalpando, J.P. Morán-Lázaro, Carbon dioxide gas sensing behavior of nanostructured $GdCoO_3$ prepared by a solution-polymerization method, J. Alloys Compd. 484 (2009) 605–611.
[5] M.A. Pena, J.L.G. Fierro, Chemical structures and performance of perovskite oxides, Chem. Rev. 101 (2001) 1981–2018.
[6] L. Jun, Z. Ling, L. Guanzhong, Activation of methane over perovskite catalysts, Ind. Eng. Chem. Res. 48 (2009) 641–646.
[7] M. James, D. Cassidy, D.J. Goossens, R.L. Withers, The phase diagram and tetragonal superstructures of the rare earth cobaltate phases $Ln_{1-x}Sr_xCoO_{3-\delta}$ (Ln = La^{3+}, $Pr^{3+}Nd^{3+}$,Sm^{3+},Gd^{3+},Y^{3+},Ho^{3+},Dy^{3+},Er^{3+}, Tm^{3+} and Yb^{3+}), J. Solid State Chem. 177 (2004) 1886–1895.
[8] C. Bernuy-Lopez*, K. Høydalsvik, M.-A. Einarsrud, T. Grande, Effect of A-site cation ordering on chemical stability, oxygen stoichiometry and electrical conductivity in layered $LaBaCo_2O_{5-d}$ double perovskite, Materials 9 (2016) 154, http://dx.doi.org/10.3390/ma9030154.
[9] H. Shiiba, C.L. Bishop, M.J.D. Rushton, M. Nakayama, M. Nogami, J.A. Kilner, R.W. Grimes, Effect of A-site cation disorder on oxygen diffusion in perovskite-type $Ba_{0.5}Sr_{0.5}Co_{1-x}Fe_xO_{2.5}$, J. Mater. Chem. A 1 (2013) 10345–10352.
[10] V.A. Dudnikov, Yu S. Orlov, S. Yu Gavrilkin, et al., Effect of gd and sr ordering in a sites of doped $Gd_{0.2}Sr_{0.8}CoO_{3-delta}$ perovskite on its structural, magnetic, and thermodynamic properties, J. Phys. Chem. C 120 (2016) 13443–13449.
[11] S.N. Vereshchagin, L.A. Solovyov, E.V. Rabchevskii, V.A. Dudnikov, S.G. Ovchinnikov, A.G. Anshits, Methane oxidation over A-site ordered and disordered $Sr_{0.8}Gd_{0.2}CoO_{3-\delta}$ perovskites, Chem. Commun. 50 (2014) 6112–6115.
[12] S.N. Vereshchagin, L.A. Solov'ev, E.V. Rabchevskii, V.A. Dudnikov, S.G. Ovchinnikov, A.G. Anshits, New method for regulating the activity of ABO_3 perovskite catalysts, Kinet. Catal. 56 (2015) 640–645.
[13] R. Liu, Y. Xuan, Y.Q. Jia, Ordering and disordering in (A'A") (B'B")O3-type perovskite compounds, Mater. Chem. Phys. 57 (1998) 81–85.
[14] L. Mogni, F. Prado, C. Jiménez, A. Caneiro, Oxygen order–disorder phase transition in layered $GdBaCo_2O_{5+}$ δ perovskite: thermodynamic and transport properties, Solid State Ionics 240 (2013) 19–28.
[15] Q. Yin, Y.S. Lin, Beneficial effect of order–disorder phase transition on oxygen sorption properties of perovskite-type oxides, Solid State Ionics 178 (2007) 83–89.
[16] Z.H. Yang, Y.S. Lin, Synergetic thermal effects for oxygen sorption and order–disorder transition on perovskite-type oxides, Solid State Ionics 176 (2005) 89–96.
[17] L.A. Solovyov, Full-profile refinement by derivative difference minimization, J. Appl. Crystallogr. 37 (2004) 743–749.
[18] K. Conder, E. Pomjakushina, A. Soldatov, E. Mitberg, Oxygen content determination in perovskite-type cobaltates, Mater. Res. Bull. 40 (2005) 257–263.
[19] Thermal analysis; differential thermal analysis; principles. DIN 51007:1994–06.

[20] F. Fujishiro, T. Hashimoto, Analysis of structural phase transition from monoclinic $Ba_2Fe_2O_5$ to cubic $Ba_2Fe_2O_{5+\delta}$, Thermochim. Acta 549 (2012) 110–115.
[21] K.-H. Illers, Die ermittlung des schmelzpunktes von kristallinen polymeren mittels wärmeflusskalorimetrie (DSC), Eur. Polym. J. 10 (1974) 911–916.
[22] P.A. Heiney, J.E. Fisher, A.R. McGhie, et al., Orientational ordering transition in solid C60, Phys. Rev. Lett. 66 (1991) 2911–2914.
[23] V.M. Egorov, Toshihiro Kuzuya, V.V. Kaminskii, Shinji Hirai, N.V. Sharenkova, Specific features of the structure of semiconducting SmS polycrystals in the homogeneity region, Phys. Solid State 54 (2012) 48–52, http://dx.doi.org/10.1134/S1063783412010106.
[24] Y.-H. Bing, A.A. Bokov, Z.-G. Ye, Diffuse and sharp ferroelectric phase transitions in relaxors, Curr. Appl. Phys. 11 (2011) S14–S21.
[25] V.V. Kirillov, V.A. Isupov, Ferroelectrics 5 (1) (1971) 3.
[26] R.L. Moreira, R.P.S.M. Lobo, Phenomenological study of diffuse phase transitions, J. Phys. Soc. Jpn. 61 (1992) 1992–1995.
[27] G.A. Malygin, Analysis of the parameters of a smeared orientational transition at 250–260 K in C-60 crystals, Phys. Solid State 43 (2001) 1989–1994.
[28] W. Känzig, Ferroelectrics and Antiferroelectrics (Academic, New York, 1957; Inostrannaya Literatura, Moscow, 1960).
[29] V.Ya. Fritsberg. Izv. Akad. Nauk SSSR, Ser. Fiz. 47 (1983) 698.
[30] M. Fisher, The Nature of Critical Points, Univ. of Colorado Press, Boulder, 1965; Mir, Moscow, 1968.
[31] G. King, P.M. Woodward, Cation ordering in perovskites, J. Mater. Chem. 20 (2010) 5785–5796.
[32] M. James, T. Tedesco, D.J. Cassidy, R.L. Withers, Oxygen vacancy ordering in strontium doped rare earth cobaltate perovskites $Ln_{1-x}Sr_xCoO_{3-\delta}$ (Ln = La, Pr and Nd; x > 0.60), Mater. Res. Bull. 40 (2005) 990–1000.
[33] V. A. Cherepanov, L.Ya. Gavrilova, N.E. Volkova, A.S. Urusova, T.V. Aksenova, E. Kiselev, Phase equilibria and thermodynamic properties of oxide systems on the basis of rare earth, alkaline earth and 3d-transition (Mn, Fe, Co) metals. A short overview of. Chimica Techno Acta. 4 (2015) 273–305.
[34] A.N. Petrov, V.A. Cherepanov, O.F. Kononchuk, L. Ya. Gavrilova, Oxygen non-stoichiometry of $La_{1-x}Sr_xCo0_{3-\delta}$ ($0 < x < 0.6$), J. Solid State Chem. 87 (1990) 69–76.
[35] A.N.V.A. Petrov Cherepanov, A.Yu. Zuev, Thermodynamics, defect structure, and charge transfer in doped lanthanum cobaltites: an overview, J. Solid State Electrochem. 10 (2006) 517–537, http://dx.doi.org/10.1007/s10008-006-0124-0 A.
[36] M. Sánchez-Andújar, M.A. Senaris-Rodriguez, Cation ordering and electrical properties of the ruddlesden-Popper $Gd_{2-2x}Sr_{1+2x}Co_2O_7$ compounds (x = 0 and 0.10), Z. Anorg. Allg. Chem. 633 (2007) 1890–1896.
[37] B. Raveau, 2.03–Ruddlesden-Popper Phases and Derivatives: Homologous Series of Transition Metal Oxides. Reference Module in Chemistry, Molecular Sciences and Chemical Engineering. Comprehensive Inorganic Chemistry II (Second Edition). From Elements to Applications. (2013), Pages 63–102. Volume 2: Transition Elements, Lanthanides and Actinides.
[38] K. Yamaura, Q. Huang, R.J. Cava, Crystal structure synthesis, electrical; and magnetic properties of the new layered cobalt oxides (Sr, Ca, Ln)$_3Co_2O_{6\pm\delta}$ (Ln = Sm, Eu, Gd, Tb, Dy, Ho, and Y), J. Solid State Chem. 146 (1999) 277–286, http://dx.doi.org/10.1006/jssc.1999.8375.
[39] D. Samaras, A. Collomb, J.C. Joubert, Determination des structures de deux ferrites mixtes nouveaux de formule $BaLa_2Fe_2O_7$ et $SrTb_2Fe_2O_7$, J. Solid State Chem. 7 (1973) 337–348.
[40] H. Jeong, T. Kim, D. Kim, K.l. Kim, Hydrogen production by the photocatalytic overall water splitting on $NiO/Sr_3Ti_2O_7$: Effect of preparation method, Int. J. Hydrogen Energy 31 (2006) 1142–1146.
[41] J. Hayd, H. Yokokawa, E. Ivers-Tiffée, Hetero-Interfaces at nanoscaled (La, Sr)$CoO_{3-\delta}$ thin-Film cathodes enhancing oxygen surface-Exchange properties, J. Electrochem. Soc 160 (2013) F351–F359.